Available online at www.sciencedirect.com
SCIENCE DIRECT
Thermochimica Acta 447 (2006) 89–100
thermochimica acta
www.elsevier.com/locate/tca

# Kinetics of reduction of iron oxides by $H_2$ Part I: Low temperature reduction of hematite

A. Pineau, N. Kanari, I. Gaballah *

*Mineral Processing and Environmental Engineering Team, LEM,[1] CNRS[2] UMR 7569, ENSG,[3] INPL,[4] BP 40, 54501 Vandœuvre, France*

Received 13 July 2005; received in revised form 6 October 2005; accepted 6 October 2005
Available online 23 November 2005

**Abstract**

This study deals with the reduction of $Fe_2O_3$ by $H_2$ in the temperature range of 220–680 °C. It aims to examine the rate controlling processes of $Fe_2O_3$ reduction by $H_2$ in the widest and lowest possible temperature range. This is to be related with efforts to decrease the emission of $CO_2$ in the atmosphere thus decreasing its green house effect.

Reduction of hematite to magnetite with $H_2$ is characterized by an apparent activation energy '$E_a$' of 76 kJ/mol. $E_a$ of the reduction of magnetite to iron is 88 and 39 kJ/mol for temperatures lower and higher than 420 °C, respectively. Mathematical modeling of experimental data suggests that the reaction rate is controlled by two- and three-dimensional growth of nuclei and by phase boundary reaction at temperatures lower and higher than 420 °C, respectively.

Morphological study confirms the formation of compact iron layer generated during the reduction of $Fe_2O_3$ by $H_2$ at temperatures higher than 420 °C. It also shows the absence of such layer in case of using CO. It seems that the annealing of magnetite's defects around 420 °C is responsible for the decrease of $E_a$.

The rate of reduction of iron oxide with hydrogen is systematically higher than that obtained by CO.


*Keywords:* Reduction; Iron oxides; Hydrogen; Carbon monoxide; Temperature

## 1. Introduction

Reduction of iron oxide is probably one of the most studied topics. This is due to the importance of iron and steel in the current and future technologies. More than 2 tonnes of carbon dioxide are generated for the production of 1 tonnes of iron metal. It is well known that $CO_2$ increases the green house effect. For these reasons, this study explores the advantages and disadvantages of using pure hydrogen for the reduction of iron oxides at low temperature.

From the industrial point of view, direct reduction of iron ores with $H_2$ or natural gases could have several technical advantages, such as:

1. replacement of the expensive metallurgical coke as reducing agent;
2. low carbon content of the produced iron;
3. generated gases are essentially composed of $H_2O$ and $H_2$, thus avoiding the release of CO and $CO_2$ and by the same token avoid the projected Ecotax.

However, reduction of iron ores with hydrogen leads to compact iron layers that could slow their reduction rate. Moreover, in some cases the produced iron is pyrophoric. Finally, and in spite of serious effort [1–3], the cost of hydrogen production is currently high.

This paper is focused on the reduction of hematite with hydrogen in the temperature range of 220–680 °C.

* Corresponding author.
[1] Laboratoire Environnement et Minéralurgie, rue du Doyen M. Roubault, BP 40, 54501 Vandœuvre Cedex, France.
[2] Centre National de la Recherche Scientifique, 3 rue Michel-Ange, 75794 Paris Cedex, France.
[3] École Nationale Supérieure de Géologie, rue du Doyen M. Roubault, BP 40, 54501 Vandœuvre Cedex, France.
[4] Institut National Polytechnique de Lorraine, 2 rue de la Forêt de Haye, 54501 Vandœuvre Cedex, France.

0040-6031/$ – see front matter © 2005 Elsevier B.V. All rights reserved.
doi:10.1016/j.tca.2005.10.004

## 2. Literature review

Reduction of hematite by hydrogen proceeds in two or three steps, under and above 570 °C, respectively, via magnetite ($Fe_3O_4$) and wüstite ($Fe_{(1-x)}O$) according to the Bell's Diagram (Fig. 1) and the following equations:

$$3Fe_2O_3 + H_2 \rightarrow 2Fe_3O_4 + H_2O \quad \text{(i)}$$

$$Fe_3O_4 + 4H_2 \rightarrow 3Fe + 4H_2O \quad \text{(ii)}$$

$$(1-x)Fe_3O_4 + (1-4x)H_2 \rightarrow 3Fe_{(1-x)}O + (1-4x)H_2O \quad \text{(iii)}$$

$$Fe_{(1-x)}O + H_2 \rightarrow (1-x)Fe + H_2O \quad \text{(iv)}$$

Generally, it is admitted that wüstite is unstable below 570 °C under thermo-dynamic equilibrium. However, as shown by Fig. 1, wüstite could be an intermediate product during the reduction of hematite by hydrogen at temperature lower than 570 °C under irreversible thermodynamic conditions.

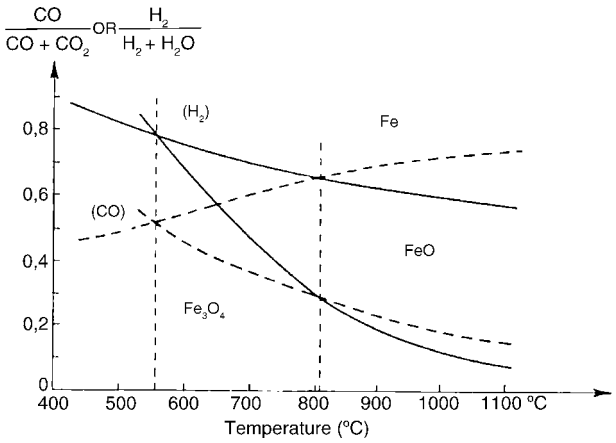


Fig. 1. Bell's Diagram for the Fe–C–O and Fe–H–O equilibrium at 1 atm.

Table 1
Apparent activation energy of the hematite reduction by hydrogen (kJ/mol)

| Parameter | Temperature range (°C) | Activation energy | Material and experimental conditions | Ref. |
|---|---|---|---|---|
| Raw material | 460–500 | 56.8 | Pure $Fe_2O_3$ | [4] |
| | 460–500 | 72.3 | Pure $Fe_2O_3$ heated to 850 °C | [4] |
| | 460–500 | 89.4 | Hematite ore | [4] |
| | 450–700 | 246.0 | $Fe_2O_3 \rightarrow Fe_3O_4$, precursor of $Fe_2O_3$was FeOOH[a] | [8] |
| | 450–700 | 93.0 | $Fe_3O_4 \rightarrow Fe$, precursor of $Fe_2O_3$ was FeOOH[a] | [8] |
| | 450–700 | 162.0 | $Fe_2O_3 \rightarrow Fe_3O_4$, precursor of $Fe_2O_3$ was ferrihydrite[a] | [8] |
| | 450–700 | 104.0 | $Fe_3O_4 \rightarrow Fe$, precursor of $Fe_2O_3$ was ferrihydrite[a] | [8] |
| Pellets | 700–925 | 109.9 | Iron ore: 80% $Fe_2O_3$, 18% FeO, globular pellets | [12] |
| | 1000–1150 | 18.0 | Iron ore: 80% $Fe_2O_3$, 18% FeO, globular pellets | [12] |
| | <500 | 30.1 and 56.4 | Ferric oxide pellets, degree of reduction ($Fe_2O_3 \rightarrow Fe_3O_4$) < 0.01, electrical conductivity | [13] |
| Step $Fe_2O_3 \rightarrow Fe_3O_4$ | 290–480 | 124.0 | $Fe_2O_3 \rightarrow Fe_3O_4$, 67% $H_2$ ($H_2$–Ar), ≈3% $H_2O$[a] | [6] |
| | 250–450 | 139.2 | $Fe_2O_3 \rightarrow Fe_3O_4$, hydrogen–argon mixture (10% $H_2$)[a] | [7] |
| | 450–700 | 246.0 | $Fe_2O_3 \rightarrow Fe_3O_4$, the precursor of $Fe_2O_3$was FeOOH[a] | [8] |
| | 450–700 | 162.0 | $Fe_2O_3 \rightarrow Fe_3O_4$, the precursor of $Fe_2O_3$ was ferrihydrite[a] | [8] |
| | 250–610 | 106.0 | $Fe_2O_3 \rightarrow Fe_3O_4$, 5% $H_2$ in He[a] | [9] |
| | 300–900 | 89.1 | $Fe_2O_3 \rightarrow Fe_3O_4$ 5% $H_2$ in $N_2$[a] | [10] |
| Step $Fe_3O_4 \rightarrow Fe$ | 290–480 | 172.0 | $Fe_3O_4 \rightarrow Fe^0$, 67% $H_2$ ($H_2$–Ar), ≈3% $H_2O$[a] | [6] |
| | 450–700 | 93.0 | $Fe_3O_4 \rightarrow Fe$, the precursor of $Fe_2O_3$ was FeOOH[a] | [8] |
| | 450–700 | 104.0 | $Fe_3O_4 \rightarrow Fe$, the precursor of $Fe_2O_3$ was Ferrihydrite[a] | [8] |
| | 250–610 | 54.0 | $Fe_3O_4 \rightarrow Fe$, 5% $H_2$ in He[a] | [9] |
| | 300–900 | 70.4 | $Fe_3O_4 \rightarrow Fe$, 5% $H_2$ in $N_2$[a] | [10] |
| $Fe_3O_4 \rightarrow Fe$ | 250–450 | 77.3 | $Fe_3O_4 \rightarrow FeO$, hydrogen–argon mixture (10% $H_2$)[a] | [7] |
| | 250–450 | 85.7 | $FeO \rightarrow Fe$, hydrogen–argon mixture (10% $H_2$)[a] | [7] |
| | 580 and 720 | 72.0 | Wüstite → Fe | [11] |
| Presence of water vapor in the reducing gas mixture | 465, 485 and 505 | 52.7 | Pure $Fe_2O_3$ with 4% water vapor (w.v.) | [5] |
| | 465, 485 and 505 | 55.2 | Pure $Fe_2O_3$ with 7.5% w.v. | [5] |
| | 465, 485 and 505 | 58.9 | $Fe_2O_3$ore with 2% w.v. | [5] |
| | 465, 485 and 505 | 53.1 | $Fe_2O_3$ ore with 5% w.v. | [5] |
| | 290–480 | 124.0 | $Fe_2O_3 \rightarrow Fe_3O_4$, 67% $H_2$ ($H_2$–Ar), ≈3% $H_20$[a] | [6] |
| | 290–480 | 172.0 | $Fe_3O_4 \rightarrow Fe$ metal, 67% $H_2$ ($H_2$–Ar), ≈3% $H_2O$[a] | [6] |
| Impurities | 460–500 | 109.9 | $Fe_2O_3$ and MgO | [4] |
| | 460–500 | 107.8 | $Fe_2O_3$ and $A1_2O_3$ or $In_2O_3$ or $Li_2O$ | [4] |
| | 460–500 | 129.2 | $Fe_2O_3$ and $TiO_2$ | [4] |
| CO | 700–1150 | 72.3 | $Fe_2O_3 \rightarrow Fe$, iron pellets cont. 97.2% of iron oxides | [12] |

[a] Temperature-programmed reduction.

Table 2
Controlling mechanisms of the iron oxides reduction

| Gas | Solid | Temperature range (°C) | Kinetics controlling mechanism | Ref. |
|---|---|---|---|---|
| $H_2$ | Pure $Fe_2O_3$ | 460–500 | Topochemical reaction at the interface gas/solid $1-(1-X)^{1/3}$ | [4] |
| | Pure $Fe_2O_3$ with 2.5–7.5% water vapor | 460–500 | Increased rate of reduction attributed to a hydrogen spill-over effect: the chemisorbed hydrogen atoms activate the surface migration | [4] |
| | Pure $Fe_2O_3$ + foreign metal oxides ($A1_2O_3$ . . .) or hematite ore | 460–500 | Retard of the reduction kinetics due to structural factor: topochemical reaction and different mechanism involving the mixed oxides ($FeAl_2O_4$ . . .) formed at the surface of $Fe_2O_3$ | [4] |
| | Pure $Fe_2O_3$ + fresh metal powders | 460–500 | Increased rate of reduction | [4] |
| | Pure $Fe_2O_3$ with water vapor | 465, 485 and 505 | The rate increases with water vapor content between 2.5 and 7.5%: this is attributed to H spill-over. The rate determining step is identified to be the desorption of $H_2O$ | [5] |
| 67% $H_2$/Ar | α-$Fe_2O_3$ (Merck, pro analysis) | 290–480 | Three-dimensional nucleation model according to Avrami–Erofeyev | [6] |
| | α-$Fe_2O_3$ (Merck, pro analysis) Addition of 3% $H_20$ to the reducing gas | 290–480 | Self-catalyzed nucleation (autocatalysis): nuclei catalyze further nuclei formation, due to branching of nuclei or to the catalytic role of the Fe metal in $H_2$ dissociation. $H_2O$ might assist during the acceleration by assuring fast hydrogen spill-over | [6] |
| 5% $H_2$/He | $Fe_2O_3$ (99.98%, Aldrich) | 250–610 | The prereduction step ($Fe_2O_3$ to $Fe_3O_4$) was described by an "nth-order" expression | [9] |
| | $Fe_2O_3$ (99.98%, Aldrich) or $Fe_3O_4$ (99.997%, Alfa Chemicals) | 250–610 | The reduction of $Fe_3O_4$ followed a nucleation or autocatalytic mechanism. Metal nuclei formed are believed to dissociate and activate dihydrogen molecules leading to autocatalysis | [9] |
| 5% $H_2$/$N_2$ | Iron oxide prepared by precipitation of | 300–900 | $Fe_2O_3 \rightarrow Fe_3O_4$ unimolecular model [a first order reaction: $r = A\exp[-E/RT](1-\alpha)$] | [10] |
| | $Fe(NO_3)_3{\cdot}9H_2O$ | 300–900 | $Fe_3O_4 \rightarrow$ Fe two-dimensional nucleation according to Avrami–Erofeyev model | [10] |
| $H_2$ | Ferric oxide pellets | <500 | For degree of reduction = $x < 0.01$: thin layer at the pellet surface has been reduced: chemisorption of $H_2$ on the oxygen vacancies | [13] |
| CO, $H_2$ | Iron ore: 80% $Fe_2O_3$, 18% FeO–globular pellets | 700–1150 | Chemical reaction: the advance of reaction front during reduction in $1-(1-R)^{1/3}$ | [12] |

One of the most important parameters of the hematite reduction is the apparent activation energy as it defines the reactor dimensions and the energy consumption. Literature survey indicates that its value depends on the starting raw material, nature of reducing gas, temperature range, reaction step, presence of water vapor in the gas mixture, impurities, physical shape, etc.

Table 1 confirms that the apparent activation energy ($E_a$) depend on these factors. $E_a$ varies from 18 to 246 kJ/mol. Such range integrates the kinetic of different controlling steps and indirectly the reactivity of solids. Moreover, Table 1 suggests that $E_a$ obtained by reducing iron oxides with CO is comparable to that of $H_2$ [4,12]. This is also confirmed by other studies [14]. Table 2 groups the controlling mechanism suggested by different

Table 3
Suggested mathematical modeling of reaction kinetics

| Equation | | Shape factor, $F_P$ | Mechanism | Ref. |
|---|---|---|---|---|
| $kt = 1-(1-X)^{1/F_P}$ | (v) | | General equation | [15] |
| $kt = X$ | (vi) | 1 | Phase-boundary-controlled reaction (infinite slabs) | |
| $kt = 1-(1-X)^{1/2}$ | (vii) | 2 | Phase-boundary-controlled reaction (contracting cylinder) | |
| $kt = 1-(1-X)^{1/3}$ | (viii) | 3 | Phase-boundary-controlled reaction (contracting sphere) | |
| $kt = X^2$ | (ix) | 1 | One-dimensional diffusion | |
| $kt = X + (1-X)\ln(1-X)$ | (x) | 2 | Two-dimensional diffusion | |
| $kt = 1-3(1-X)^{2/3} + 2(1-X)$ | (xi) | 3 | Three-dimensional diffusion | |
| $kt = [1-(2/3)X] - (1-X)^{2/3}$ | (xii) | 3 | Three-dimensional diffusion (Ginstling–Brounshtein equation) | [16] |
| $kt = [1-(1-X)^{1/3}]^2$ | (xiii) | 3 | Three-dimensional diffusion (Jander equation) | [16] |
| $kt = [-\ln(1-X)]$ | (xiv) | 1 | Random nucleation; unimolecular decay law (first-order) | [16] |
| $kt = [-\ln(1-X)]^{1/2}$ | (xv) | 2 | Two-dimensional growth of nuclei (Avrami–Erofeyev equation) | [16] |
| $kt = [-\ln(1-X)]^{1/3}$ | (xvi) | 3 | Three-dimensional growth of nuclei (Avrami–Erofeyev equation) | [16] |

Where $k$ is the constant, $t$ the reduction time (min), $X$ the extent of reduction ($X = 0$ at the beginning of the reduction and $X = 1$ at the end of reduction) and $F_P$ the particle shape factor (1 for infinite slabs, 2 for long cylinders and 3 for spheres).

authors for the iron oxides at different temperature ranges. It is clear that the controlling mechanism is related to the starting raw material, gas composition, temperature range, etc. Table 3 presents the suggested equations used for the mathematical modeling of the kinetic data of the reaction. Eqs. (v)–(xvi) cover most of the probable mechanisms that control the gas–solid reactions. These equations will be used for the mathematical modeling of our kinetic data. The best fitting equation(s) will be chosen to eventually determine the controlling mechanism.

## 3. Material and experimental procedure

Hematite used in this study had a $Fe_2O_3$ content higher than 99.8% supplied by Merck. Impurities are essentially traces of $Ca^{2+}$, $Mg^{2+}$, $Cl^-$ and $SO_4^{2-}$. The specific surface area of $Fe_2O_3$ was 0.51 $m^2$/g. The porosity volume is 3.3 $cm^3$/g. The SEM indicates that the grain size of the hematite is about 1–2 μm.

Thermogravimetric (TG) tests were performed using 100 mg of sample and a CAHN microbalance (Fig. 2). It has a sensibility of 20 μg. The sample is reduced in gold boat having a surface area of about 2.2 $cm^2$. The sample was first heated in a nitrogen flow to the desired temperature. $N_2$ was then replaced by preheated $H_2$ at the initial reduction time. The average velocity of $H_2$ was about 3 cm/s and the flow rate was about 100 1/h. A data acquisition system records the sample weight and temperature as a function of time. Hematite, as well as the reduction products, were examined by X-rays diffraction (XRD) and scanning electron microscope (SEM).

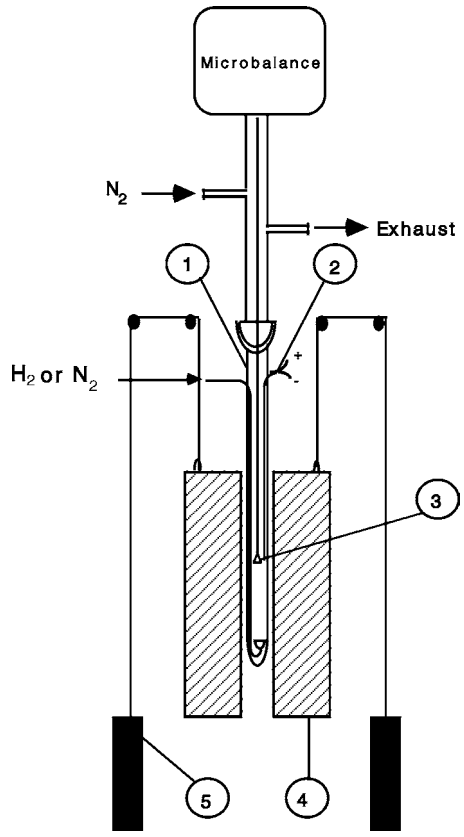


Fig. 2. Thermogravimetric apparatus. (1) Quartz reactor, (2) thermocouple, (3) sample boat, (4) furnace and (5) counterweight.

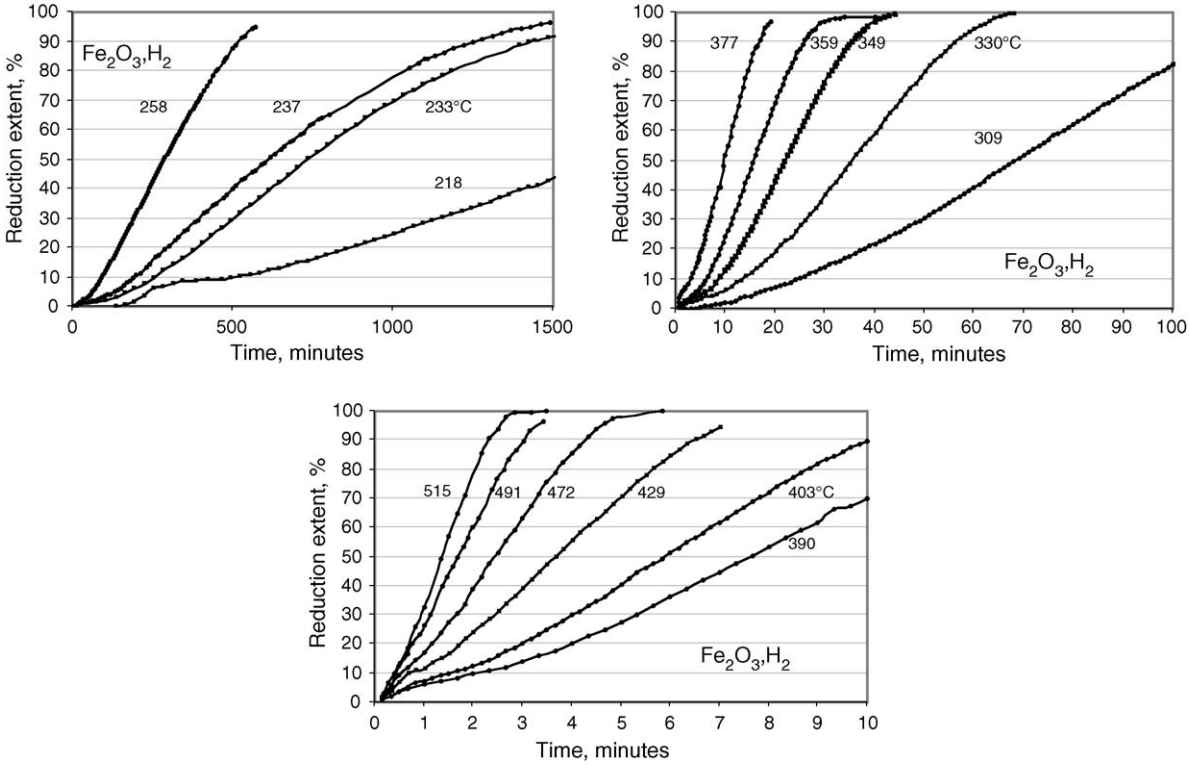


Fig. 3. Evolution of reduction extent percentage vs. reaction time for the reduction of hematite with hydrogen.

## 4. Results

Fig. 3 groups the isotherms of hematite reduction versus the reaction time at different temperatures. As can be observed, most of the isotherms have a plateau at about 11% of reduction extent percentage '*R*%' that corresponds to the reduction of hematite to magnetite. One may underline that the time for full reduction of hematite is about 1500, 40 and 5 min at temperatures 237, 349 and 472 °C, respectively. This suggests that the apparent activation energy '$E_a$' is relatively important. Fig. 4 is the Arrhenius diagram obtained by using the data of Fig. 3.

This figure shows that the value of $E_a$ for the reduction of hematite to magnetite is about 76 kJ/mol. The reduction of magnetite to iron is characterized by an apparent activation energy of 88 and 39 kJ/mol at temperatures lower and higher than 417 °C, respectively.

Fig. 5 groups the mathematical modeling of the experimental data during the reduction step of $Fe_3O_4$–Fe with $H_2$ at 233, 330 and 472 °C. The models tested for the temperatures generates correlation coefficient that varies from 0.9921 to 0.9993. It is almost arbitrary to choice between these models. However, it seems that the best fitting of data obtained at 233 and 330 °C is that of Eqs. (xv) and (xvi). These equations suggest that the reaction is controlled by the two- and three-dimensional growth of nuclei. This mechanism is in agreement with the value of $E_a$ at temperatures < 417 °C. At 472 °C, the best fitting of experimental data is obtained using Eq. (vi). This equation suggests that reduction of magnetite at this temperature is controlled by phase boundary reaction (infinite slabs).

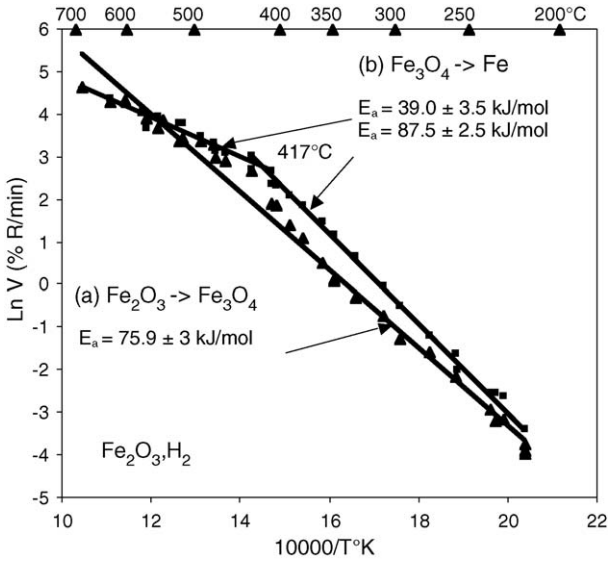


Fig. 4. Arrhenius diagram for the reduction of hematite by hydrogen. (a) Reduction extent ≤ 11% and (b) reduction extent ≥ 11%.

Fig. 6 exhibits the morphological aspects of the reduction products at different temperatures using the SEM. Pictures A–C indicate that the average grain size is almost constant. At temperatures higher than 425 °C, pictures D and E show gradual sintering of grains. This could explain the modification of $E_a$ and the change in the mechanism controlling the reaction rate. However, Eq. (vi) could be explained by gas starvation. For this

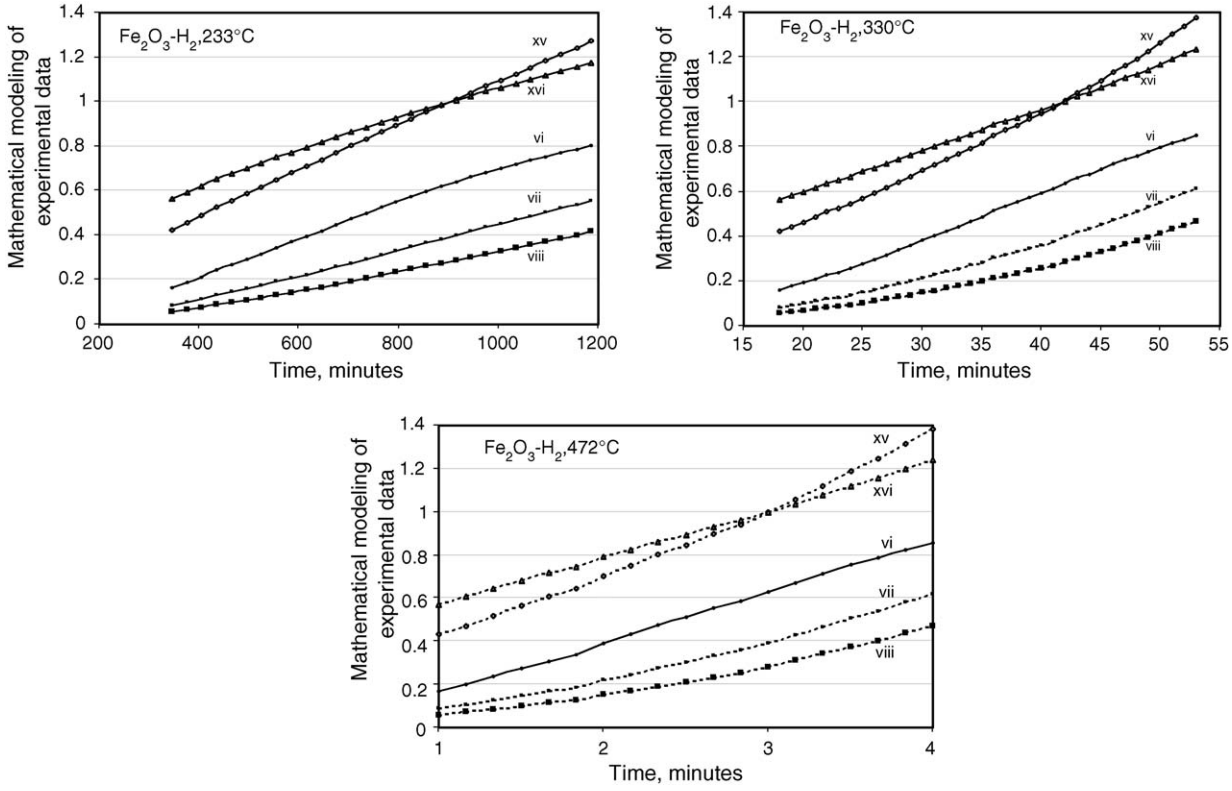


Fig. 5. Mathematical modeling of experimental data of Fig. 3. (—) Correlation coefficients > 0.995 and (- - -) correlation coefficients < 0.995

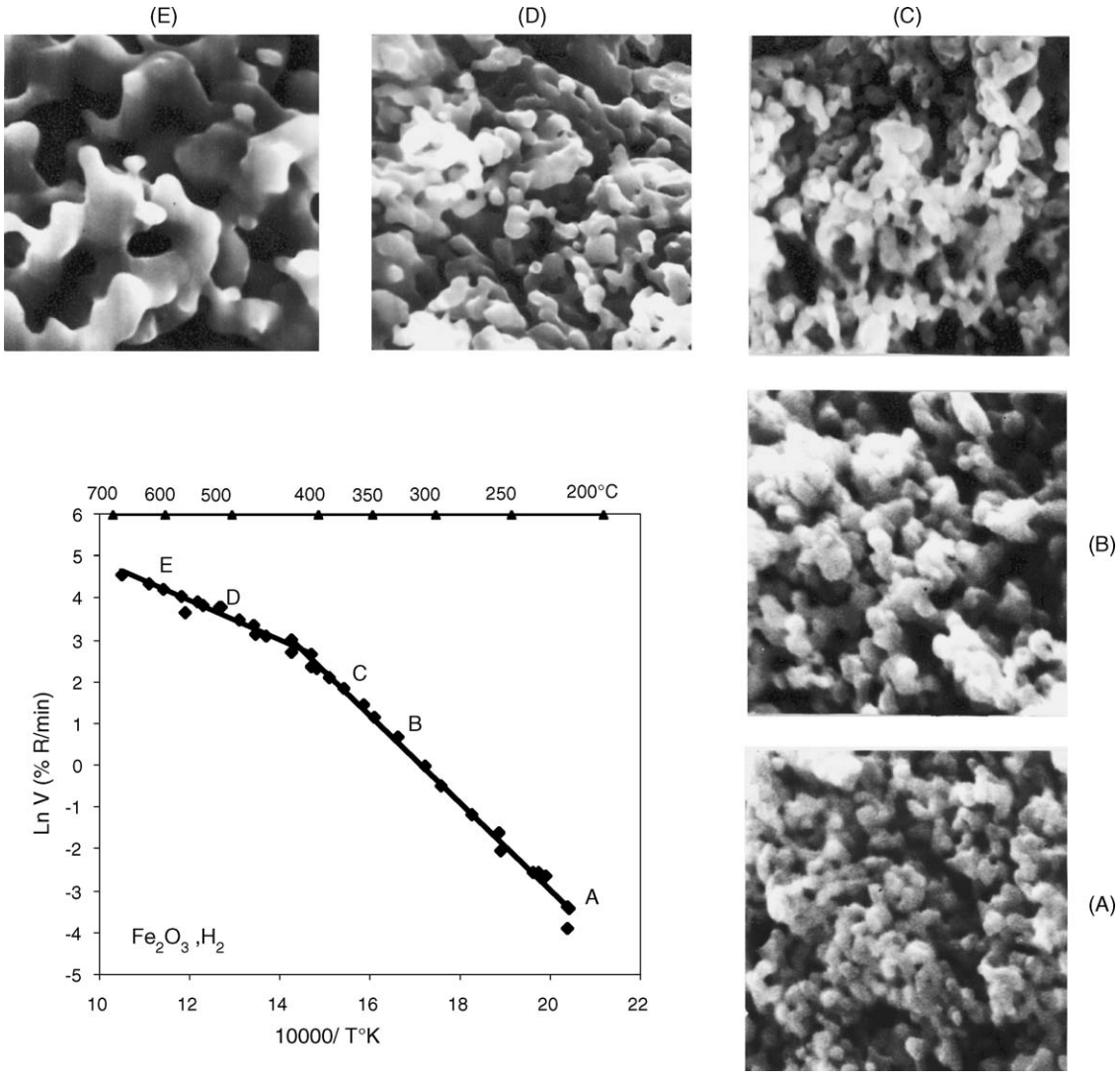


Fig. 6. Effect of reduction temperature on the morphological aspects of reduction products using hydrogen ($X = 6000 \pm 600$).

reason, reduction of hematite is studied using a gas mixture composed of 10% $H_2$ and 90% $N_2$.

Fig. 7 traces the evolution of $R$% as function of time at different temperatures for the reduction of hematite with the above mentioned gas mixture. At 586 °C, the curve shows two plateaus at $R$% of about 11 and 33. These values correspond to the reduction of $Fe_2O_3$ into $Fe_3O_4$ and $Fe_3O_4$ into $Fe_{(1-x)}O$, respectively.

At lower temperatures, only the plateau at 11% reduction extent is observed that corresponds to the reduction of hematite to magnetite. Fig. 8 shows the Arrhenius plot of Fig. 7 data. Again, a change of $E_a$ occurs at about 415 °C confirming results of the hydrogen reduction of hematite (Fig. 4). On the other hand, the value of $E_a$ decreases from about 103 to 36 kJ/mol as the reduction temperature exceeds that of the transition temperature ($T_t$) 415 °C. Mathematical analysis of Fig. 7 data confirms that the reaction rate, at temperature lower than $T_t$, is controlled by the two- and three-dimensional growth of nuclei and by phase boundary reaction at higher temperature.

Fig. 9 reflects the morphological aspects of hematite reduction with the gas mixture $H_2$–$N_2$ at temperature lower and higher than $T_t$. Again, it is clear that sintering of particles is performed at temperature higher than 415 °C.

It is well known that the hydrogen reduction of iron oxides produces a compact iron layer [6,8,10,12]. Consequently, the decrease of the apparent activation energy could be attributed to the formation of this compact layer of iron that slow down the reaction rate leading to lower $E_a$. To check this hypothesis, experimentation of the hematite reduction with carbon monoxide is performed.

Fig. 10 shows the evolution of the reaction extent versus time for the reduction of hematite by CO at different temperatures. One may underline that the weight increase corresponds to the formation of iron carbide. Only data of the initial reaction rate are used to calculate the evolution of the reaction rate as function of $1/T$ (K). Results are grouped in Fig. 11. This figure shows that $E_a$ for the reduction of $Fe_2O_3$ to $Fe_3O_4$ is about 114 kJ/mol. While the reduction of magnetite to iron is characterized by an $E_a$ of 114 and 40 kJ/mol at temperatures lower and higher than 439 °C, respectively.

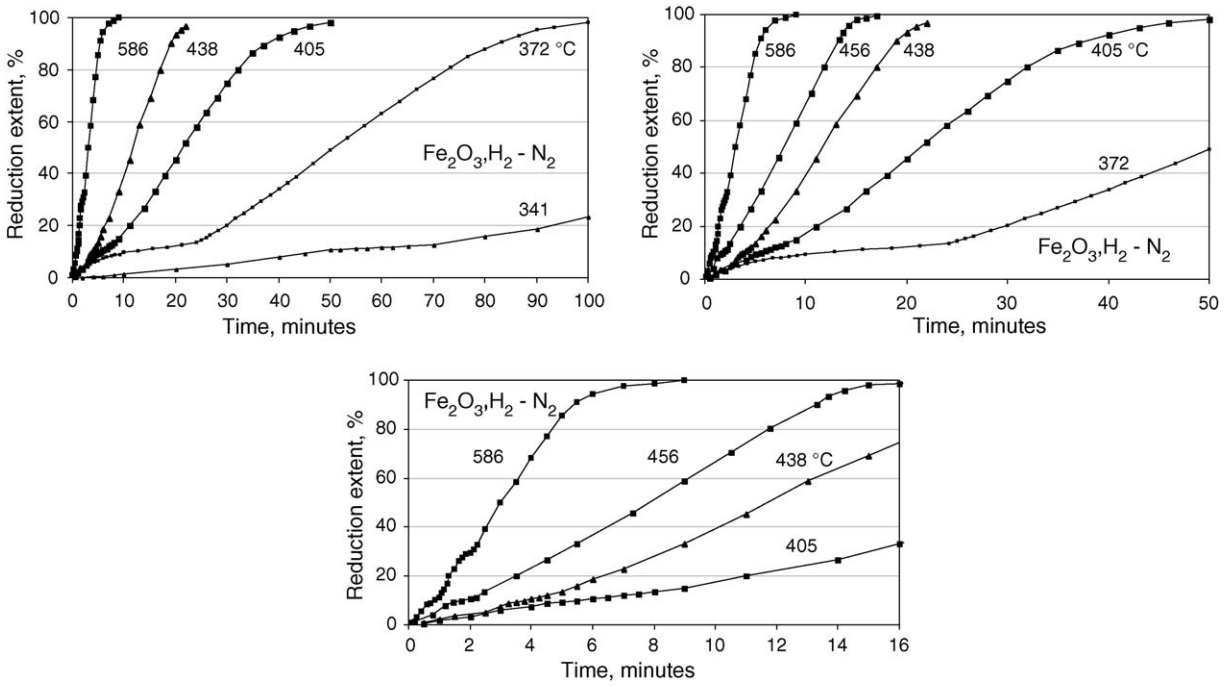


Fig. 7. Evolution of reduction extent percentage vs. reaction time for the reduction of hematite with hydrogen–nitrogen.

Fig. 12 shows the evolution of the morphological aspects of the reaction products of the reduction of $Fe_2O_3$ by CO. It seems that sintering of the particles is avoided in this case. One may come to the conclusion that the compact iron layer could be responsible for the modification of the reaction rate expressed by the decrease of $E_a$. However, Fig. 11 also shows a transition temperature of about 439 °C. Consequently, the hypothesis about the influence of the compact layer of $Fe^0$ on decrease of $E_a$ can be abandoned. Thus, it is probable that other physico-chemical phenomenon is responsible of this evolution.

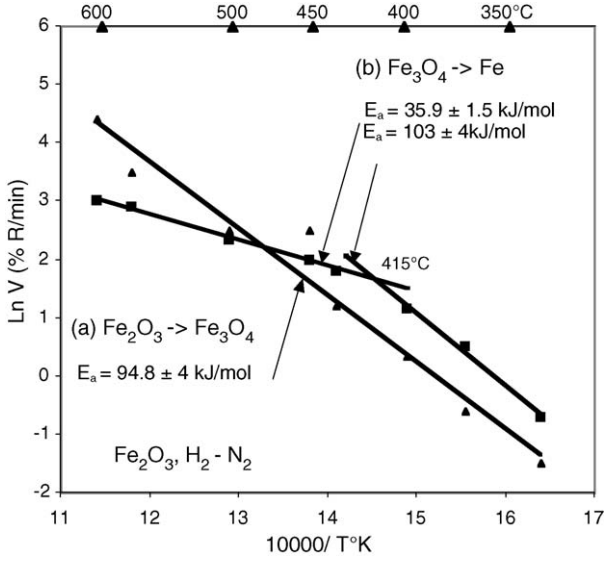


Fig. 8. Arrhenius diagram for the reduction of hematite by $H_2$–$N_2$. (a) Reduction extent ≤ 11% and (b) reduction extent ≥ 11%.

To check this hypothesis, a X-rays furnace is used for the in situ reduction of hematite with hydrogen. This furnace allows data collection of formed solids for $\theta = 0$–$60°$. The goniometer speed was adapted to the reaction kinetics at different temperatures and varied from $\theta$ equal 0.25–1°/min. Details of this furnace are grouped in Ref. [17].

Eq. (xvii) summarizes the obtained results, from X-ray diffraction, using gas mixtures containing $H_2$ and $N_2$. While results at temperatures lower than 450 °C and higher than 570 °C are expected, that obtained in the temperature range of 450–570 °C revels the presence of wüstite. Moreover, wüstite's crystal parameter, in this temperature range, was about 4.33 Å corresponding to almost stoechiometric FeO. One may underline that the presence of wüstite at temperatures lower than 570 °C have been detected by other authors [18,19].

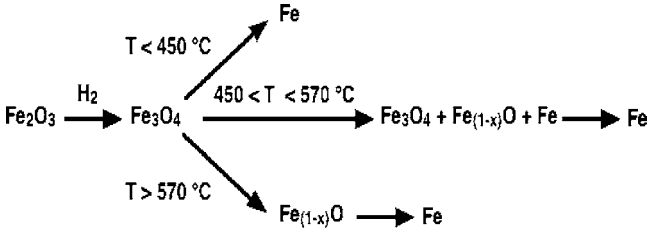


(xvii)

Consequently, the decrease of $E_a$ around $T_t$ could be explained by the different paths during the magnetite reduction. At temperatures lower than $T_t$ reduction of magnetite produces directly metallic iron. Between $T_t$ and 570 °C, reduction of $Fe_3O_4$ leads to the formation of wüstite and metallic iron. At temperatures higher than 570 °C, reduction of magnetite to $Fe^0$

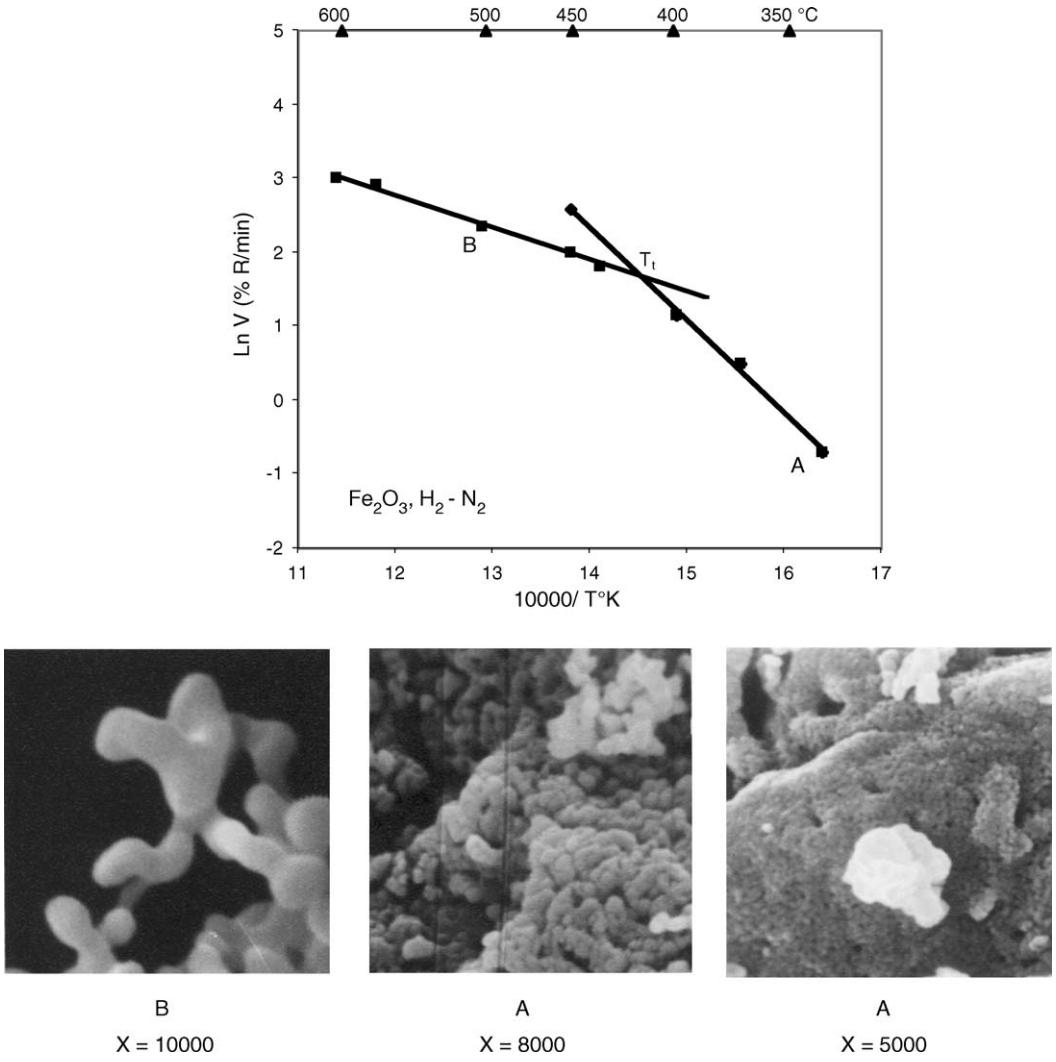


Fig. 9. Effect of reduction temperature on the morphological aspects of reduction products using a gas mixture $H_2$–$N_2$.

proceeds through the intermediate formation of wüstite. One may correlate $T_t$ to the formation of wüstite. This imposes the question why $Fe_{(1-x)}O$ appears in this temperature range? Tentative response will be discussed in Section 5.

Fig. 13 groups the data of the reduction of $Fe_3O_4$ by $H_2$ and $H_2 + N_2$. This figure confirms that the values of $E_a$ and $T_t$ are comparables. Consequently, the hypothesis of gas starvation can be neglected. However, $T_t$ for the reduction of $Fe_3O_4$ by CO is equal to 439 °C. One may underline that this is probably due to the cementation of $Fe^0$. Consequently, the data used for the calculation of $E_a$ as well as the transition temperature are limited to 20% of the reaction extent generated by the reduction of magnetite to iron using CO. As a result, the real reaction rate of the reduction of $Fe_3O_4$ by CO could be higher than the obtained values. Consequently, the value of $E_a$ should be higher than the reported one and $T_t$ should be lower than the calculated one. Fig. 14 compares data obtained by the reduction of $Fe_3O_4$ by $H_2$ and CO. This figure emphasizes that the rate of reduction of magnetite with hydrogen is higher than that obtained using CO.

## 5. Discussion

As indicated in Table 1, $E_a$ depend on the raw material and its purity and the physical state of this raw material. Moreover, for the same solid, different experimental conditions leads to different values of $E_a$. Several authors confirm these conclusions as indicated in Table 4. Results obtained in this work agreed with those of Refs. [9,10,20,23,24]. The suggested mechanisms of reduction of hematite match with those of Refs. [6,9,10]. On the other hand, the evolution of $E_a$ versus the temperature shows, in some cases, an important decrease of the apparent activation energy around a transition temperature as shown in Table 5. Several authors suggested that such evolution is due to change of the gas–solid reaction from the chemical regime at low temperature to mixed or diffusion regime at high temperatures [20,21,26–29,39,40].

However, this evolution can also be attributed to Hedvall effect [33–35] that relates the change of reactivity of solids to first and second order transitions. In some cases $T_t$ corresponds to a magnetic transformation such as Curie temperature

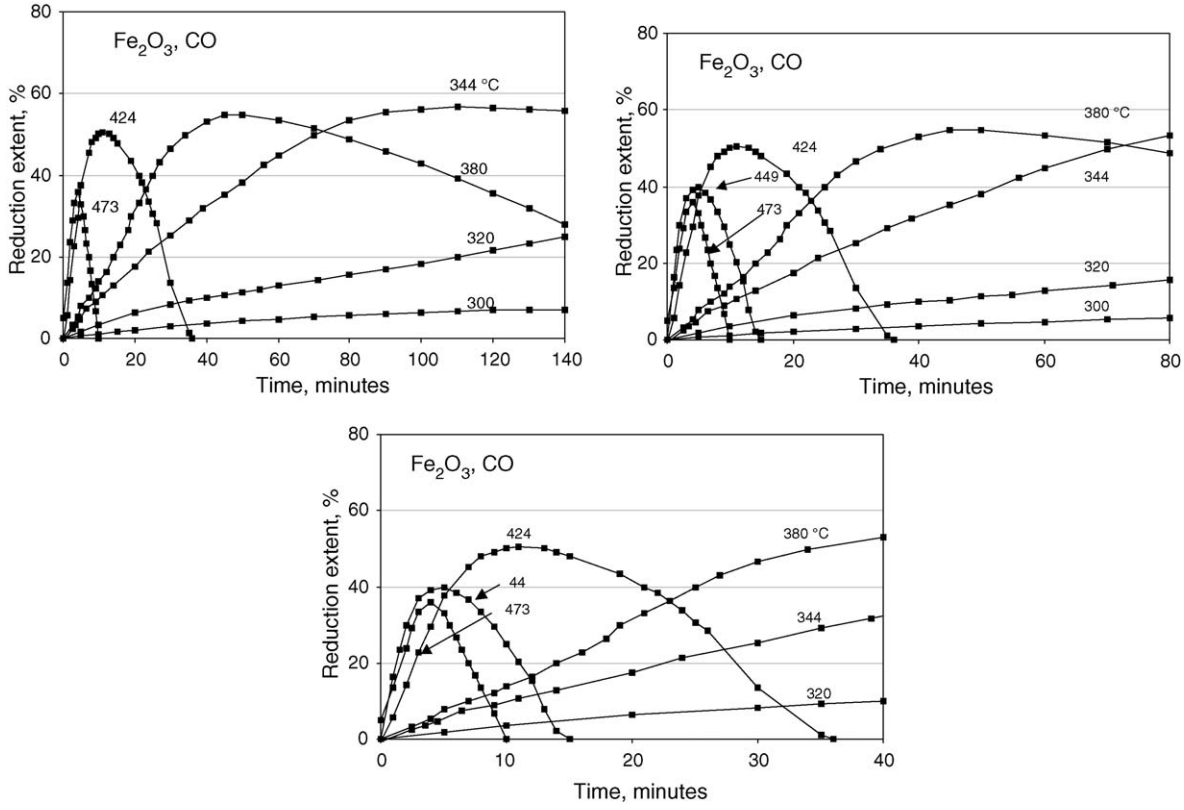


Fig. 10. Evolution of reaction extent percentage vs. reaction time for the reduction of hematite with CO.

(575 °C for $Fe_3O_4$ [36]) or phase transition such as that of α-Fe to γ-Fe (906 °C) [37,38]. However, most of $T_t$ of Table 5 does not correspond to any physical transitions of the concerned solids.

To elucidate the decrease of $E_a$ around the transition temperature, the following experimental parameters have been modified:

1. sample weight from 10 to 100 mg;
2. concentration of $H_2$ in the reducing gas mixture from 10 to 100%;
3. nature of the reducing gas: $H_2$ or CO;
4. gas velocity from about 2 to 4 cm/s;
5. boat's material (Cu or Au);
6. experimental method TGA and in situ XRD.

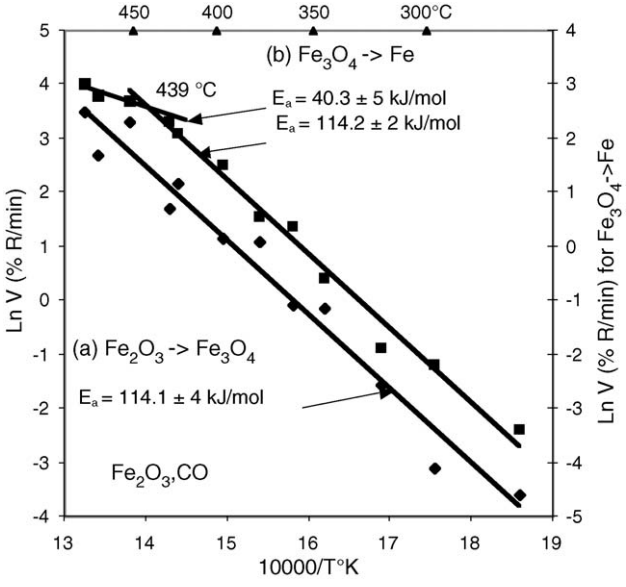


Fig. 11. Arrhenius diagram for the reduction of hematite by CO. (a) Reaction extent ≤ 11% and (b) reaction extent ≥ 11%.

Performing the above mentioned modifications of experimental parameters leads to almost the same results. In situ XRD between 300 and 700 °C revels the presence of stoechiometric wüstite at about 450 °C. In this case, one may suggest that $T_t$ is more or less independent of all the above-mentioned experimental parameters and could be related to the presence of wüstite or other physico-chemical phenomenon.

Naeser and Scholz [41] examined the effect of grinding on the reduction of hematite by hydrogen. They observed that the reduction of the ungrounded sample starts at 420 °C. While that of the ground one starts at 340 °C. This is probably due to increase of the solids' defects through mechanical treatment. Papanastassiou and Bitsianes [27] studied the oxidation of magnetite to hematite and found that $E_a$ decreases sharply at temperature higher than 400 °C. Schrader and Vogelsberger [42] indicate the presence of two exothermic peaks around 250 and 400 °C during the oxidation of magnetite to hematite. They attributed these peaks to the oxidation of $Fe_3O_4$ to γ-$Fe_2O_3$ and transformation of γ-$Fe_2O_3$ to α-$Fe_2O_3$, respectively. They also indicate that the second peak's temperature is variable. It depends on the initial hematite sample's state of deformation.

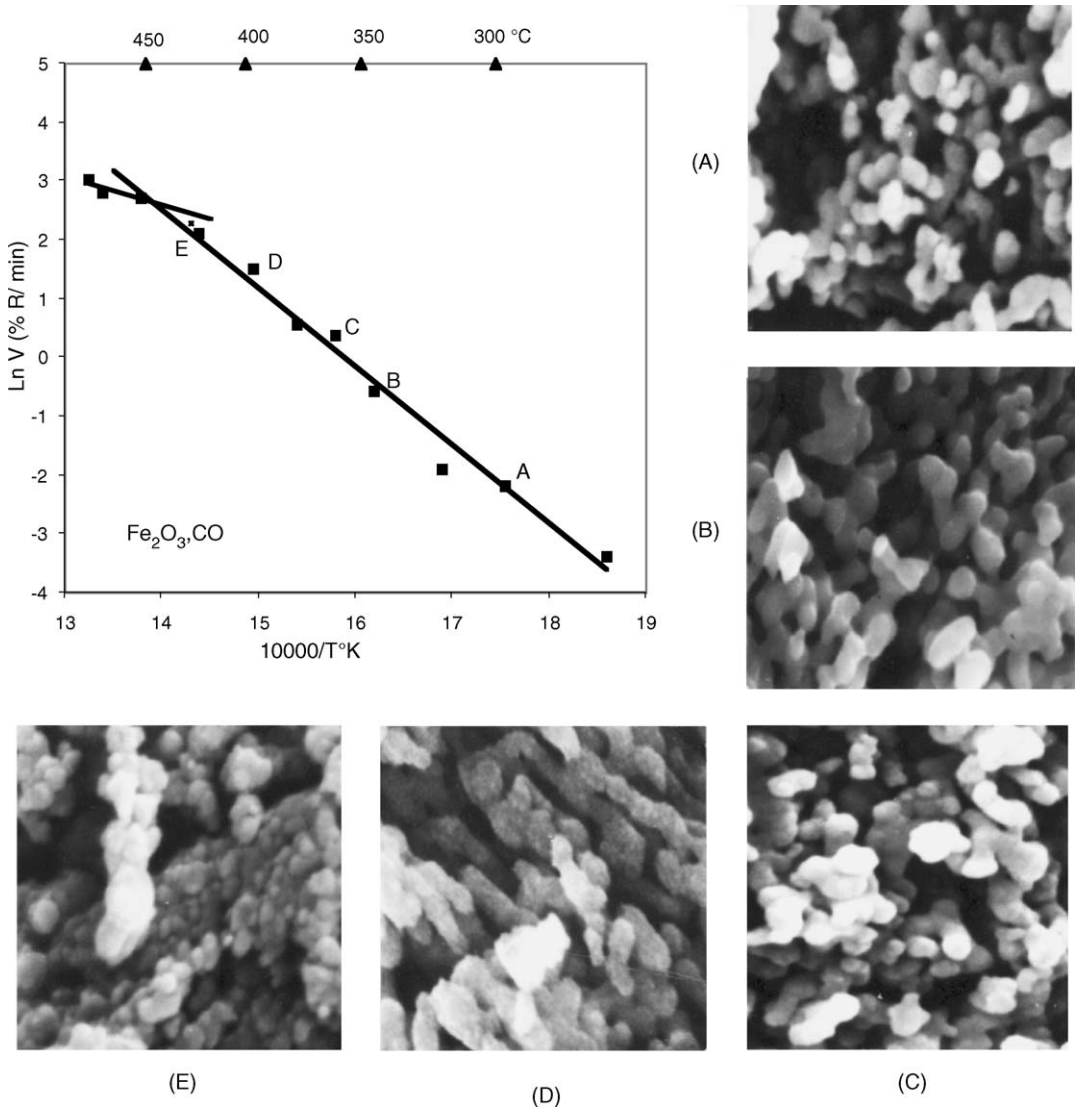


Fig. 12. Effect of reduction temperature on the morphological aspects of reduction products using CO ($X = 7000 \pm 700$).

Table 4
$E_a$ in relation with the starting material, temperature range and the reducing gas mixture

| Ref. | Step | Temperature range (°C) | Gas | $E_{a1}$ (kJ/mol) | $T_t$ (°C) | $E_{a2}$ (kJ/mol) |
|---|---|---|---|---|---|---|
| [20] | $Fe_2O_3 \rightarrow Fe$ | 400–1000 | $H_2$ | 51.0 | 575 | 38.0 |
| [20][a] | $Fe_2O_3 \rightarrow Fe$ | 400–1000 | $H_2$ | 96.1 | 575 | 48.9 |
| [21] | $Fe_2O_3 \rightarrow Fe$ | 400–1050 | $H_2$–$N_2$ | 62.3 | 550 | 64.0 |
| [22] | $Fe_3O_4 \rightarrow Fe$ | 400–900 | $H_2$ | 61.4 | 550–600 | 13.4 |
| [23] | $Fe_2O_3 \rightarrow Fe_2O_3 + Fe_3O_4 + Fe$ | 250–400 | $H_2$ | 62.7 | | |
| [23] | $Fe_2O_3 \rightarrow Fe_3O_4$ | 250–400 | $H_2$ or CO | 108.7 | | |
| [23] | $Fe_2O_3 \rightarrow Fe_3O_4$ | 250–400 | $H_2$ | 108.7 | | |
| [24] | $Fe_2O_3 \rightarrow Fe_3O_4$ | 254–298 | $H_2$ | 125.4 | | |
| [24] | $Fe_2O_3 \rightarrow Fe_3O_4$ | 210–254 | CO | 125.4 | | |
| [25] | $Fe_2O_3 \rightarrow Fe_3O_4$ | 290–360 | $H_2$ | 137.9 | | |
| This work | $Fe_2O_3 \rightarrow Fe_3O_4$ | 220–683 | $H_2$ | 75.9 | | |
| This work | $Fe_2O_3 \rightarrow Fe_3O_4$ | 337–604 | $H_2$–$N_2$ | 94.8 | | |
| This work | $Fe_2O_3 \rightarrow Fe_3O_4$ | 265–482 | CO | 114.1 | | |
| This work | $Fe_3O_4 \rightarrow Fe$ | 220–683 | $H_2$ | 88.0 | 417 | 39 |
| This work | $Fe_3O_4 \rightarrow Fe$ | 337–604 | $H_2$–$N_2$ | 103.0 | 415 | 36 |
| This work | $Fe_3O_4 \rightarrow Fe$ | 265–482 | CO | 114.0 | 439 | 40 |

[a] Natural single crystals (Sweden).

Table 5
Evolution of $E_a$ around $T_t$ for different solid–gas reactions

| Ref. | Starting solid | Process | Method | Product | $E_{al}$[a] | $T_t$ (°C)[b] | $E_{a2}$[c] |
|---|---|---|---|---|---|---|---|
| [26] | $WO_{2.9}$ | Reduction | TGA | W | 94.0 | 625 | 37.6 |
| [20] | $Fe_2O_3$ | Reduction | TGA | Fe | 96.1 | 575 | 48.9 |
| | $Fe_2O_3$ | Reduction | TGA | Fe | 50.2 | 575 | 37.6 |
| [22] | $Fe_3O_4$ | Reduction | TGA | Fe | 61.4 | 550 | 13.4 |
| [27] | $Fe_3O_4$[d] | Oxidation | TGA | $Fe_2O_3$ | 164.7 | 390 | 10.0 |
| | $Fe_3O_4$[e] | Oxidation | TGA | $Fe_2O_3$ | 143.4 | 420 | 10.5 |
| [28] | $Fe_2O_3$ | Reduction | TGA | $Fe_3O_4$ | 61.2 | 441 | 7.3 |
| [29] | Fe | Chlorination | TGA | $FeCl_2$ | 96.1 | ~400 | ~21.0 |
| [30] | Nb | Oxidation | TGA | $NbO_2$ | ~96.0 | 400 | ~21.0 |
| [31] | $Cu_2O$ | Oxidation | TGA | CuO | ~54.3 | ~765 | <54.3 |
| [32] | Cu | Sulfidation | TGA | $Cu_2S$ | 71.1 | ~400 | 34.3 |

[a] $E_{a1}$: apparent activation energy ($E_a$) for $T < T_t$.
[b] $T_t$: transition temperature.
[c] $E_{a2}$: $E_a$ for $T > T_t$.
[d] Missouri–magnetite concentrate.
[e] Taconite concentrate.

Gillot et al. [43] confirmed the existence of the two peaks and show that their temperature is function of the grains' size. They indicate that the temperature of the transition γ-$Fe_2O_3$ to α-$Fe_2O_3$ decreases from 470 °C, for solids of average grain size of 600 Å, to 380 °C for solids having an average grain size of 1400 Å.

All these authors suggest that the reactivity of solids is influenced by their imperfections. Fagherazzi and Lanzavecchia [44] have confirmed this hypothesis as they indicated that magnetite annealed at 500 °C gets rid of its defects and part of its microdeformation.

Fox and Soria-Ruiz [45] studied the effect of dislocations movement on the kinetics of thermal decomposition of freshly cleaved calcite crystal. They found two patterns of behavior at temperatures lower and higher than 427 °C. They attributed this change to the fast annealing of crystal's defects at temperatures higher than 427 °C.

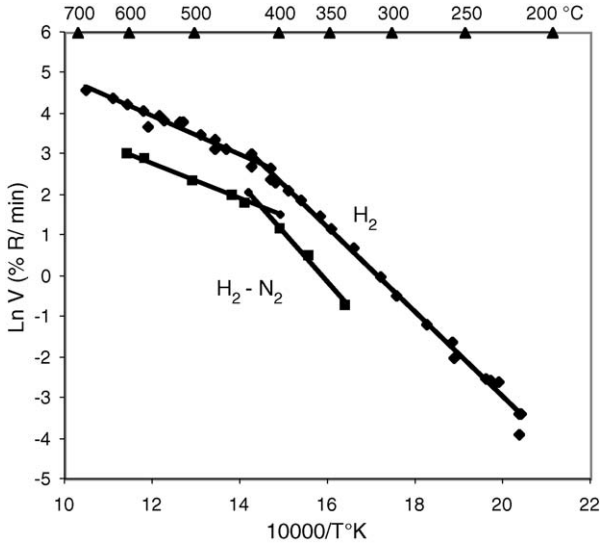


Fig. 13. Arrhenius diagrams for the reduction of hematite by $H_2$ and $H_2$–$N_2$ for a reduction extent ≥ 11% corresponding to the reduction of $Fe_3O_4 \rightarrow Fe^0$.

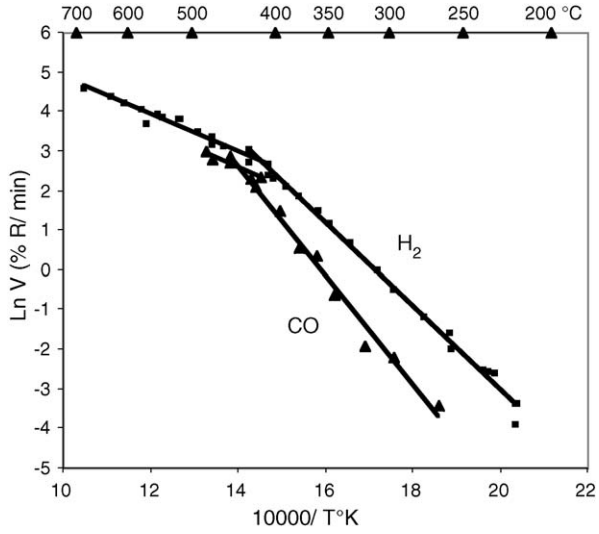


Fig. 14. Arrhenius diagrams for the reduction of hematite by $H_2$ and CO for a reduction extent ≥ 11% corresponding to the reduction of $Fe_3O_4 \rightarrow Fe^0$.

Dabosi [46], Venturello et al. [47], Hu [48] and Leslie [49] observed a reduction of the dislocation density of metallic iron in the temperature range of 400–450 °C. They attributed this phenomenon to the recovery and/or re-crystallization of iron.

In absence of studies on behavior of dislocations in iron oxides in function of temperature and with respect to results of several authors [41–49], one may speculate that $T_t$ could be related to the annealing of the magnetite defects around 420 °C. Consequently, the formation of stoechiometric wüstite, as intermediate in the reduction of $Fe_3O_4$ to $Fe^0$, is probably due to upgrading of the crystal structure.

## 6. Conclusions

Results of the reduction of iron oxides with hydrogen in the temperature range of 200–680 °C leads to the following conclusions:

1. The reduction of hematite in magnetite by $H_2$ is characterized by an apparent activation energy of about 76 kJ/mol.
2. The reduction path of magnetite to iron is function of the reaction temperature. At temperatures lower than 420 °C, $Fe_3O_4$ is reduced directly to iron. At $450 < T < 570$ °C, magnetite and wüstite are present with iron. At $T > 570$ °C, magnetite is fully reduced to wüstite before its reduction to Fe.
3. The apparent activation energy for the reduction of $Fe_3O_4$ by $H_2$ decreases from 88 to 39 kJ/mol for temperatures lower and higher than 420 °C.
4. Mathematical modeling of experimental data suggest that the controlling mechanism is the two- and three-dimensional growth of nuclei and by phase boundary reaction at higher temperature.
5. The decrease of $E_a$ around 420 °C could be attributed to the annealing of defects of the crystalline structure of magnetite.
6. The reduction rate of magnetite with hydrogen is higher than that obtained with CO.
7. The morphological study of the reduced samples of iron oxides by $H_2$ shows agglomeration of the reaction product at temperatures higher than 420 °C. Reduction of these oxides with CO does not generate compact iron layer.

In spite of results obtained in this work, low temperature reduction of iron oxides with hydrogen is handicapped by lack of data about the behavior of point and linear defects of iron oxides as function of temperature that control its reactivity, the high energy consumption and cost of hydrogen production.

## Acknowledgments

Part of this work was performed in 'Laboratoire de Chimie du Solide' of the University of Nancy, France. The authors thank Dr. Ch. Gleitzer for his help and discussions. They also indebted to Mrs. Ch. Richard for her kind help in technical and administration work.

## References

[1] Anonymous, Hydrogen production, in: US Climate Change Technology Program—Technology Options for the Near and Long Term, November, 2003, p. 75.
[2] L. Barreto, A. Makihira, K. Riahi, Int. J. Hydrogen Energy 28 (2003) 267.
[3] A. Carlson, Energy Policy 31 (2003) 951.
[4] M.V.C. Sastri, R.P. Viswanath, B. Viswanathan, Adv. Hydrogen Energy 2 (1981) 1279 (Hydrogen Energy Prog. 3).
[5] B. Viswanathan, R.P. Viswanath, M.V.C. Sastri, Trans. Indian Inst. Metals 32 (4) (1979) 313.
[6] O.J. Wimmers, P. Arnoldy, J.A. Moulijn, J. Phys. Chem. 90 (1986) 1331.
[7] G. Munteanu, L. Ilieva, D. Andreeva, Thermochim. Acta 291 (1997) 171.
[8] G. Munteanu, L. Ilieva, D. Andreeva, Thermochim. Acta 329 (2) (1999) 157.
[9] M.J. Tierman, P.A. Barnes, G.M.B. Parkes, J. Phys. Chem. B 105 (2001) 220.
[10] H.Y. Lin, Y.W. Chen, C. Li., Thermochim. Acta 400 (1–2) (2003) 61.
[11] A. Jess, H. Depner, Steel Res. 69 (3) (1998) 77.
[12] E. Mazanek, M. Wyderko, Met.-Odlew. Met. (1974) 55.
[13] M.H.A. Elhamid, M.M. Khader, A.E. Mahgoub, B.E.L. Anadouli, B.G. Ateya, J. Solid State Chem. 123 (2) (1996) 249.
[14] (a) N. Rudenko, S.T. Rostovtsev., Izv. V.U.Z. 4 (1959) 3;
(b) O.L. Koxtelov, S.T. Rostovtsev., Sta. 3 (1965) 209.
[15] J. Szekely, J.W. Evans, H.Y. Sohn., Gas-Solid Reactions, Academic Press, New York, 1976, p. 115, 232.
[16] A. Ortega, Thermochim. Acta 284 (1996) 379.
[17] N. Gerard, J. Phys. E Sci. Instrum. 5 (1972) 524.
[18] V.P. Romanov, P.A. Tatsienko, L.F. Checherskaya, G.P. Basantsev, V.D. Checherskii, Izv. Akad. Nauk SSSR, Neorganischeskie Materialy 7 (3) (1971) 450.
[19] V.P. Romanov, L.F. Checherskaya, P.A. Tatsienko, Phys. Stat. Sol. A 15 (1973) 721.
[20] N.B. Gray, J. Henderson, TMS-AIME 236 (1966) 1213.
[21] W.M.M.C. Kewan, TMS-AIME 218 (1960) 2.
[22] J.M. Quets, M.E. Wadsworth, J.R. Lewis, TMS-AIME 218 (1960) 545.
[23] U. Colombo, F. Gazzarrini, G. Lanzavecchia, Mater. Sci. Ing. 2 (1967) 125.
[24] V.A. Roiter, V.A. Yuza, A.N. Kuzentsov, Zhur. Fiz. Khim. 25 (8) (1951) 960.
[25] D. Dobovisek, B. Korousic, Rudarsko-Metalurski Zbornik (2) (1968) 127.
[26] L.C. Dufour. Thesis, Dijon, 1965.
[27] D. Papanastassiou, G. Bitsianes, Met. Trans. 4 (1973) 487.
[28] J.P. Hansen, G. Bitsianes, T.L. Joseph, B.F. Coke Oven and Raw Mater. Conference (1960) 185.
[29] R.J. Fruehan, Met. Trans. 3 (1972) 2585.
[30] E.A. Gulbransen, K.F. Andrew, J. Electrochem. Soc. A (1958) 105.
[31] K. Hauffe, P. Kofstad, Z. Elektrochem. 59 (1955) 399.
[32] A. Galerie, M. Caillet, J. Besson, in: J. Wood, et al. (Eds.), 8th ISRS, Gothenburg 14-19/6/1976, Plenum Press, 1977.
[33] J.A. Hedvall, Z. Anorg, Allgem. Chem. 61 (1924) 135.
[34] (a) H. Forestier, R. Lille, Comp. Rend. 204 (1937) 265, 1254;
(b) H. Forestier, R. Lille, Comp. Rend. 208 (1939) 891.
[35] H. Forestier, M. Daire, Akad. der Wissenschaftenundder Lit. (7) (1966) 705.
[36] A. Chakraborty, J. Magn. Magn. Mater. 204 (1999) 57.
[37] I. Gaballah, F. Jeannot, Ch. Gleitzer, C.R. Acad. Sci. Ser. C 280 (1975) 697.
[38] I. Gaballah, C. Gleitzer, J. Aubry, in: J. Wood, et al. (Eds.), Reactivity of Solids, Plenum Press, 1977, p. 391.
[39] E. Wicke, Chemie–Ingenieur Technic 29 (1957) 305.
[40] L. Bonnetain, G. Hoyant, Les Carbones, Masson, Paris, 1965, tome II, 290 pp.
[41] G. Naeser, W. Scholz, Kolloid-Zeitschrift 156 (1) (1958) 1.
[42] R. Schrader, W. Vogelsberger, Z. Chem. 9 (9) (1969) 354.
[43] B. Gillot, J. Tyranowicz, A. Rousset, Mater. Res. Bull. 10 (1975) 775.
[44] G. Fagherazzi, G. Lanzavecchia, Mater. Sci. Eng. 5 (2) (1970) 63.
[45] P.G. Fox, J. Soria-Ruiz, Proc. R. Soc. Lond. A 314 (1970) 429.
[46] F. Dabosi. Thesis, Paris, 1962.
[47] C. Venturello, C. Antonione, F. Bonaccorso, Trans. AIME 227 (1963) 1433.
[48] H. Hu, Recovery and Recrystallization of Metals, Interscience, New York, 1963, p. 311.
[49] W.C. Leslie, Recrystallization, grain growth and textures, Am. Soc. Met. (1967) 59.